PREDICTION OF EVAPOTRANSPIRATION IN THE PAMPEAN PLAIN FROM CERES SATELLITE PRODUCTS AND MACHINE LEARNING TECHNIQUES
Facundo Carmona et al.
Meteorologica, Vol. 48 Nº2 (2023), e021, julio-diciembre 2023
ISSN 1850-468X — https://doi.org/10.24215/1850468Xe021
https://revistas.unlp.edu.ar/meteorologica/index
Centro Argentino de Meteorólogos
Buenos Aires - Argentina

PREDICTION OF EVAPOTRANSPIRATION IN THE PAMPEAN PLAIN FROM CERES SATELLITE PRODUCTS AND MACHINE LEARNING TECHNIQUES

Facundo Carmona[1,2], Adán Faramiñán[1,2], Raúl Rivas[2,3], Facundo Orte[1,4]

[1]Consejo Nacional de Investigaciones Científicas y Técnicas (CONICET)
[2]UE CONICET - Instituto de Hidrología de Llanuras "Dr. Eduardo Jorge Usunoff"
[3]Comisión de Investigaciones Científicas de la Provincia de Buenos Aires (CICPBA)
[4]CEILAP-UNIDEF (CITEDEF-CONICET)

(Manuscrito recibido el 22 de marzo de 2022, en su versión final el 17 de agosto de 2022)

ABSTRACT

A key aspect in agricultural zones, such as the Pampean Plain of Argentina, is to accurately estimate evapotranspiration rates to optimize crops and irrigation requirements and the floods and droughts prediction. In this sense, we evaluate six machine learning approaches to estimate the reference and actual evapotranspiration (ET_0 and ET_a) through CERES satellite products data. The results obtained applying machine learning techniques were compared with values obtained from ground-based information. After training and validating the algorithms, we observed that Support Vector machine-based Regressor (SVR) showed the best accuracy. Then, with an independent dataset, the calibrated SVR were tested. For predicting the reference evapotranspiration, we observed statistical errors of MAE = 0.437 mm d^{-1}, and RMSE = 0.616 mm d^{-1}, with a determination coefficient, R^2, of 0.893. Regarding actual evapotranspiration modelling, we observed statistical errors of MAE = 0.422 mm d^{-1}, and RMSE = 0.599 mm d^{-1}, with a R^2 of 0.614. Comparing the results obtained with the machine learning models developed another studies in the same field, we understand that the results are promising and represent a baseline for future studies. Combining CERES data with information from other sources may generate more specific evapotranspiration products, considering the different land covers.
Keywords: Evapotranspiration, CERES, Machine Learning, Teledetection.

PREDICCIÓN DE LA EVAPOTRANSPIRACIÓN EN LA REGIÓN PAMPEANA POR MEDIO DE DATOS CERES Y TÉCNICAS DE APRENDIZAJE AUTOMÁTICO

RESUMEN

Un aspecto clave en zonas agrícolas, como la llanura Pampeana argentina, es poder estimar con precisión las tasas de evapotranspiración para optimizar cultivos y requerimientos de riego, como así también la predicción de inundaciones y sequías. En este sentido, se evaluaron seis algoritmos de aprendizaje automático para estimar la evapotranspiración de referencia y la evapotranspiración real (ET_0 y ET_a, respectivamente) utilizando productos de satélite CERES como datos de

Dirección Electrónica: facundo.carmona@rec.unicen.edu.ar

entrada. Los valores modelados, aplicando técnicas de aprendizaje automático, se compararon con aquellos obtenidos a partir de información de terreno. Después de entrenar y validar los algoritmos, observamos que el Regresor con Vectores de Soporte (SVR) mostraba la mejor precisión. A continuación, con un conjunto de datos independiente, se testearon los algoritmos SVR calibrados. Para la predicción de la evapotranspiración de referencia se observaron errores estadísticos de MAE = 0.437 mm d^{-1} y RMSE = 0.616 mm d^{-1}, con un coeficiente de determinación R^2 = 0.893. Por otro lado, al predecir la evapotranspiración real, observamos errores estadísticos de MAE y RMSE de 0.422 mm d^{-1} y 0.599 mm d^{-1}, respectivamente, con un R^2 de 0.614. Al comparar los resultados obtenidos con los algoritmos de aprendizaje automático con aquellos arrojados por estudios en la misma área, entendemos que los resultados aquí mostrados son prometedores y representan una línea de base para futuros trabajos. La combinación de datos de CERES con información de otras fuentes puede generar productos de evapotranspiración más específicos, considerando además las diferentes coberturas del suelo.
Palabras clave: Evapotranspiración, Aprendizaje Automático, CERES, Teledetección.

1. INTRODUCTION

Climate change alters the complex interplay between land and atmosphere, significantly impacting different processes in the global hydrological cycle (Martens et al., 2018). Evapotranspiration (ET) is a significant component of the hydrological cycle and one of the most important physical processes in natural ecosystems. It explains the exchange of water and energy between the soil, land surface, and the atmosphere (Jing et al., 2019; Ochoa-Sánchez et al., 2019; Chia et al., 2020a).

ET is used widely in many fields such as agronomy, hydrology, climatology, and environmental science (Miralles et al., 2011; Xiang et al., 2020). It represents an important indicator for the management and planning of water resources, and for such a reason, its estimation is essential in the study of hydrological processes. In this sense, physically-based indirect methods arise from the difficulty of obtaining field measurements precisely using several equations to estimate the evapotranspiration rates from meteorological data. Such is the case of the FAO-56 Penman-Monteith method (FAO56-PM) for estimating reference evapotranspiration (ET_0), which is recommended for irrigation scheduling worldwide because it generally shows the best results under various climatic conditions (Nema et al., 2017; Xiang et al., 2020). Accurate calculations of ET_0 are the prerequisite for obtaining the upper limit on crop water requirements (potential crop evapotranspiration) and the fundamental basis for formulating agricultural irrigation systems (Lewis and Allen, 2017). However, the conditions encountered in the field differ generally from the "standard conditions" defined in the FAO-56 Penman-Monteith requirements (Allen et al., 1998). The effects of soil water stress reduce the evapotranspiration rates (non-standard conditions), and its consideration allows to obtain the actual evapotranspiration, ET_a. Therefore, monitoring the total available water by computing the daily water balance for the root zone is needed.

On the other hand, due to advances in remote sensing technology and methods, numerous models were developed to obtain evapotranspiration products with satellite data that can offer unique spatial-temporal variations. Remote sensing technology appears to remove the limitation of spatial coverage when estimating ET (Chia et al., 2020b).

Methods based on satellite data include: i) energy balance methods; ii) methods based on the relationship between vegetation index and surface temperature; iii) methods based on the Penman-Monteith equation; iv) methods based on the Priestley-Taylor equation; v) empiric methods and vi) soil water balance methods (Zhang et al., 2016; Carmona et al., 2018; Degano et al., 2020). In this sense, the estimation of ET crucial, especially when dealing with agricultural regions, such as the Pampean Region of Argentina (PRA). In fact, there is a growing development of application methods to estimate the evapotranspiration in the PRA (Walker et al., 2018; Carmona et al., 2018; Degano et al., 2020).

Machine learning techniques are increasingly being considered for ET estimation at different scales, including remote sensing data. When adequate and reliable experimental data are available, a promising alternative approach for estimating evapotranspiration rates is provided by machine learning algorithms, which are particularly suited to address non-linear regression problems depending on many variables (Granata et al., 2020). Artificial Intelligence (AI) based approaches have emerged as an alternative solution to map the relationships between meteorological parameters and evapotranspiration, even with limited knowledge of the real interactions between variables (Chia et al., 2020b). Among several machine learning models, evolutionary computing has demonstrated a remarkable progression in the modelling of ET_0. In this sense, Jing et al. (2019) presented an interesting review of the implementation of evolutionary computing models to estimate ET_0 employing meteorological data (2007–2019). There are few examples of AI methods applying remote sensing data in comparison with those that use meteorological data. Yang et al. (2006) proposed a model predicting continental-scale evapotranspiration by combining Moderate Resolution Imaging Spectrometer (MODIS), AmeriFlux data and support vector machine technique (RMSE = 0.62 mm d^{-1}, and R^2 = 0.75). Lu and Zhuang (2010) developed an artificial neural networks model to estimate the daily evapotranspiration (R^2 = 0.52 - 0.86), using remote sensing data from the MODIS, meteorological data, and eddy covariance flux data. Chen et al. (2013) developed an artificial neural network model from AmeriFlux data, and land surface products derived from remote sensing data (R^2 = 0.77, and RMSE = 0.62 mm d^{-1}). Zhang et al. (2018) explored three machine learning algorithms (support vector machine, back-propagation neural network, and an adaptive neuro-fuzzy inference system) for estimating ET_0 from remote sensing data. Their results suggest that the land surface temperature (LST) could be used to accurately estimate ET_0 with high correlation coefficients (R^2 = 0.897 - 0.915) and show that the surface reflectance data slightly improve the model's accuracy.

The National Weather Service (SMN, for its acronym in Spanish) of Argentina has a weather stations network that allows estimating the evapotranspiration and validating related satellite products. From the information provided by the SMN and other meteorological stations, the Agricultural Risk Office (ORA, for its acronym in Spanish) of Argentina works to monitor the soil water reserve in grasslands and cultivation areas. ORA provides the values of ET_0 from meteorological data and ET_a estimations from water balance computation on the root zone.

In this study, we propose to use CERES (Clouds and the Earth's Radiant Energy System) satellite products data as input variables and Machine Learning techniques for estimating evapotranspiration in the PRA. We train and test several techniques, particularly linear regression methods, decision trees, among others, and an artificial neural network for predicting ET_0 and ET_a with CERES products data. Ground data provided by the ORA were used to train, validate, and test the machine learning algorithms.

2. MATERIALS AND METHODS

2.1. Study area and ground data

PRA is an extensive and fertile plain of approximately 600,000 km^2 that encompasses several Argentine provinces. This region presents low elevation, and typical regional topographic gradients (<0.1 %). It is located within the region of subtropical and mid-latitudes or temperate climates, characterized by long periods of drought and floods, which affect the availability of water, and the productivity of agricultural systems, among other human activities. According to Aliaga et al. (2017), the climate in PRA can be divided into eight climate zones: Continental (C), Subtropical (ST), Temperate Highland of Ventania Hills (THVH), Temperate Oceanic (TO), Temperate Very Humid (TVH), Warm-Highland of Pampean Hills (WHPH), Warm-humid (WH), and Semiarid (SA). ET_0 and ET_a values calculated by the ORA were used from this broad region. These measurements are based on information from 24 sites placed in seven climate zones of the PRA, as depicted in Fig. 1 and Table 1. Due to a lack of quality information, the SA zone was not considered.

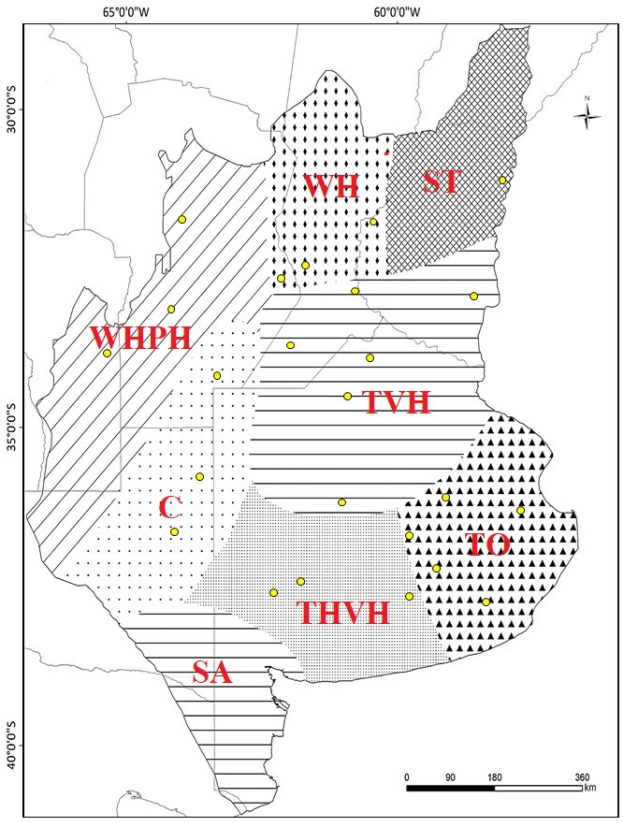

Figure 1: Pampean Region of Argentina, climates zones (in red text and different weft patterns), and spatial distribution of the meteorological stations used (yellow points) (modified from Aliaga et al. (2017)).

2.2. Reference crop evapotranspiration

The ET_0 values were estimated by ORA from the FAO56-Penman-Monteith method (Allen et al., 1998):

$$ET_0 = \frac{0{,}408\Delta(Rn - G) + \gamma\left(\frac{900}{T_m+273}\right)u_2(e_s - e_a)}{\Delta + \gamma(1 + 0{,}34u_2)} \quad (1)$$

where ET_0 is the daily reference crop evapotranspiration in mm d^{-1}, Δ is the slope of the saturation vapour pressure-temperature curve (kPa C^{-1}), Rn is the net radiation (MJ m^2 d^{-1}), G is the soil heat flux (MJ m^2 d^{-1}), is the psychrometric constant (kPa C^{-1}), Ta is the daily mean air temperature (^{o}C), u_2 is the mean daily wind speed at 2 m (m s-1), e_s is the saturation vapour pressure (kPa), and e_a is the actual vapor pressure (kPa).

2.3. Actual evapotranspiration

The ET_a was calculated by ORA with a soil water balance method. It consists of assessing the incoming and outgoing water flux into the vegetation root zone over some time period. ET_a can be deduced from the change in soil water storage over time (Eq.2) (Allen et al., 1998; Degano et al., 2021). The daily water balance used to calculate soil water storage considers the following terms:

The ET_0 values were estimated by ORA from the FAO56-Penman-Monteith method (Allen et al., 1998):

$$S_f + Ex_f = S_i + Ex_i + P - RO - DP - ET_a \quad (2)$$

where S_f and S_i are the final and initial soil water storage, Ex_f and Ex_i are the final and initial excess water accumulated on the surface, P is the rainfall, RO is the surface runoff, and DP is the deep percolation. Subsurface horizontal movements of water have been neglected, generally of a lower order than the vertical ones. Soil moisture content can be at its maximum retention capacity or field capacity (in which the extraction of water by the vegetation occurs without any difficulty), or it can drop to values below the permanent wilting point, in which the vegetation is it would wither without resilience even in a saturated atmosphere. The difference between wilting point and field capacity is the available water. The ability of a soil to store water depends on the amount and size of its pores, that is, on its structure, texture, and content of organic matter. When soil moisture is less than field capacity, the ET_a is less than its potential value. It decreases as the level of water stress to which the vegetation is subjected increases. Finally, ET_a can be obtained from potential crop evapotranspiration, and the initial soil storage is expressed as a fraction of the field capacity (Degano et al., 2021).

2.4. CERES products

As input variables within machine learning algorithms, CERES_SYN1deg_Ed3A satellite products available at the CERES website (http://ceres.larc.nasa.gov) were used (Rutan et al., 2015, NASA/LARC/SD/ASDC, 2017). The "SYN"(Synoptic Radiative Fluxes and Clouds) means that this version provides radiation data on clear and all-sky conditions, the "1deg" means it has a 1-degree spatial resolution, and the "Ed3A" is the version number (Smith et al., 2011; Jia et al. 2016). Considering that the main driving forces on the ET process are available energy, aerodynamic effects, and soil water storage (for ET_a), we chose as input variables the CERES products mentioned in Table 2. The solar radiation ($Rs_{\downarrow}$) and incoming longwave radiation ($Rl_{\downarrow}$) represent the radiative term that provides the available energy to the soil-water-plant system. The T_{skin} is proportional to the energy output from the system, increasing when the evaporative fraction is reduced due to a less water availability in the soil. The auxiliary data W (as an indicator of the water available in the atmosphere) and u_{10} represent the aerodynamic terms in the evapotranspiration process, and the atmospheric pressure (p_{atm}) influences the psychrometric constant. In addition, the theoretical solar radiation ($Rs_{\downarrow 0}$) indicates the maximum solar radiation available due to cloud-less conditions. As the solar radiation varies throughout the year, it also gives us information about the time of the year in the study area. Geographic location also was considered in the machine learning algorithms.

2.5. Machine learning algorithms

Multilayer Perceptron (MLP), Random Forest (RF), Support vector machine-based regressor (SVR), XGBoost regressor (XGBR), Generalized Linear Models (GLM), and K-Nearest Neighbor regressor (KNN) algorithms were selected in order to compare each performance. These were executed using the Scikit-learn library in Google Colaboratory (COLAB). Scikit-learn is a Python module for machine learning built on top of SciPy and is distributed under the 3-Clause BSD license (Pedregosa et al., 2011), and COLAB is a free online cloud-based Jupyter notebook environment that allows to train machine learning and deep learning models.

MLP is an artificial neural network that optimizes the squared loss using LBFGS or stochastic gradient descent. It consists of three types of layers. The input layer receives the input signal to be processed. The output layer performs the required task such as prediction and classification. An arbitrary number of hidden layers placed between the input and output layer are the accurate computational engine of the MLP. As a feed-forward network in a MLP, the data flow from the input to the output layer (Kisi, 2007; Kisi, 2008; Landeras et

Station	*Climate zone*	*Lat* (°)	*Lon* (°)	*Altitude* (m)	*T* (°C)	*RH* (%)	*u10* (km h-1)	*P* (mm y-1)
Concordia	ST	-31.2	-58.0	38	18.9	72	9.3	1377
Paraná	WH	-31.8	-60.5	87	18.2	72	11.3	1148
Gualeguaychú	TVH	-33.0	-58.6	21	17.9	74	9.5	1119
Pilar	WHPH	-31.7	-63.9	338	17.1	69	8.9	797
Marcos Juárez	WH	-32.7	-62.2	110	17.0	75	10.5	912
Río Cuarto	WHPH	-33.1	-64.1	421	16.4	67	15.7	859
Villa Reynolds	WHPH	-33.7	-65.4	486	15.6	70	11.4	706
Junín	TVH	-34.6	-60.9	81	16.0	73	12.1	1044
Bolívar	TVH	-36.2	-61.1	93	15	68	14.9	967
Venado Tuerto	TVH	-33.7	-62.0	113	16.9	66	13.5	978
Laboulaye	C	-34.1	-63.4	137	15.9	72	10.6	903
El Trébol	WH	-32.5	-61.7	96	18.2	65	13.5	1004
Rosario	TVH	-32.9	-60.8	25	17.5	74	11.4	1022
Pergamino	TVH	-33.9	-60.6	65	17.1	68	14.2	1080
Las Flores	TO	-36.1	-59.1	38	15.2	71	14.8	1011
Dolores	TO	-36.3	-57.7	9	14.9	79	9.6	928
Azul	TO	-36.8	-59.8	147	14.5	71	15.2	960
Tandil	TO	-37.2	-59.3	175	13.5	75	13.3	879
Balcarce	TO	-37.8	-58.3	120	14.0	73	16.9	934
Coronel Suárez	THVH	-37.4	-61.9	233	13.5	72	15.6	806
Pigüé	THVH	-37.6	-62.4	304	13.6	69	11.1	612
Benito Juárez	THVH	-37.7	-59.8	207	13.7	70	16.9	909
General Pico	C	-35.7	-63.8	145	16.2	69	12.0	863
Santa Rosa	C	-36.6	-64.3	191	15.5	66	10.0	746

Table I: Station city, climate zone, geographic location, and weather characteristics of the sites used. T: Mean annual air temperature, RH: Relative Humidity, u_{10}: wind speed at 10 m, P: Rainfall. Climate data from SMN of Argentina (period 1981–2010).

al., 2008; Izadifar and Elshorbagy, 2010; Abbe et al., 2022). RF regressor is an ensemble method that combines the predictions from multiple decision trees on various sub-samples of the dataset to make a more accurate prediction than the individual models (Breiman, 2001; Ok et al., 2012; da Silva Júnior et al., 2019). SVR uses the same principles as the support vector machine for classification. The basic idea behind SVR is to find the best fit line. The best fit line is the hyperplane with the maximum number of points (Kisi and Cimen, 2009; Fan et al., 2018; Chia et al., 2020a; Faramiñán et al., 2021). XGBR is a decision tree-based ensemble algorithm that uses a gradient boosting framework. It works as Newton-Raphson in function space unlike gradient boosting which works as gradient descent in function space, a second-order Taylor approximation is used in the loss function to make the connection to Newton Raphson method (Chen and Guestrin, 2016). The idea behind boosting is to generate multiple "weak"prediction models sequentially, and each of these takes the results of the previous model to generate a "stronger" model, with better predictive power and greater stability

Variable	*Description*	*Source*	*Units*
$Rs_{\downarrow}$	Shortwave Flux Down, All-sky conditions	CERES	W m^{-2}
$Rs_{\downarrow 0}$	Shortwave Flux - Down, Clear-sky conditions	CERES	W m^{-2}
$Rl_{\downarrow}$	Longwave Flux Down, All-sky conditions	CERES	W m^{-2}
T_{skin}	Skin Temperature	CERES	K
p_{atm}	Surface pressure	CERES - Auxiliary Data	hPa
W	Total Column Precipitable Water	CERES - Auxiliary Data	cm
u_{10}	Wind Speed at 10 m	CERES - Auxiliary Data	m s^{-1}
lat , lon	Latitude and Longitude	center location of CERES pixel	degrees

Table II: Variables, descriptions, sources, and units of the CERES products used.

in its results (Chen and Guestrin, 2016; Han et al., 2019; Putatunda and Rama, 2018). Finally, GLM expands the general linear model. The dependent variable is linearly related to the factors and covariates via a specified link function (Faramiñan et al., 2022). And KNN makes a prediction based on the local interpolation of the targeted variable in the k-nearest neighbours (Yamaç and Todorovic, 2020).

2.6. Methodology

The flowchart in Figure 2 depicts the methodology used to evaluate the machine learning models and find the best models. The first step was to establish a connection with the databases. Considering the CERES products data for each exact location of the validation sites and the ET_0 and ET_a values provided by the ORA, we elaborated a data set of 22 columns x 119,729 rows, where each column represents a variable (response or exploratory) or a data type, and each row represents a daily mean value of each variable from 2000 to the 2013 year. The next step was to prepare the data as input to the machine learning regression algorithms. The whole dataset was pre-processed and split into training, validation, and testing. The data for the period 2000-2009 (∼70 % of whole dataset) was used as training and validation dataset. A random split 80/20 training/validation on 2000-2009 dataset was employed to find the best configuration for each model (MLP, RF, SVR, XGBR, GLM and KNN algorithms). The remaining data for the period 2010-2013 (∼30 % of whole dataset) was reserved as testing dataset. The models were trained using different variables sets of CERES products as input. After analyzed the accuracy of each model using the validation dataset, the testing dataset was then used to evaluated the performance of the previous models (Results in Table 3). Finally, the performance of the best models developed with daily data for both ET_0 and ET_a, is evaluated in; i) different climate zones (Results in Table 4), ii) different temporal scales (averaged 8, 16 and 30 days, Results in Table 5).

2.7. Performance metrics

Three typical metrics were used in this study to assess the performance of the retrieved models. Also, a plot of observations against the predicted values illustrates how the points match the 1:1 line to evaluate each model's performance. The scatter plot allows for a visual inspection of each model's performance (performance is better the closer the values are to the line). The Root-mean-square error (RMSE) and the mean absolute error (MAE) were used to evaluate the models' errors. The RMSE has been used as a standard statistical metric to measure model performances in meteorology, air quality, and climate research studies. The

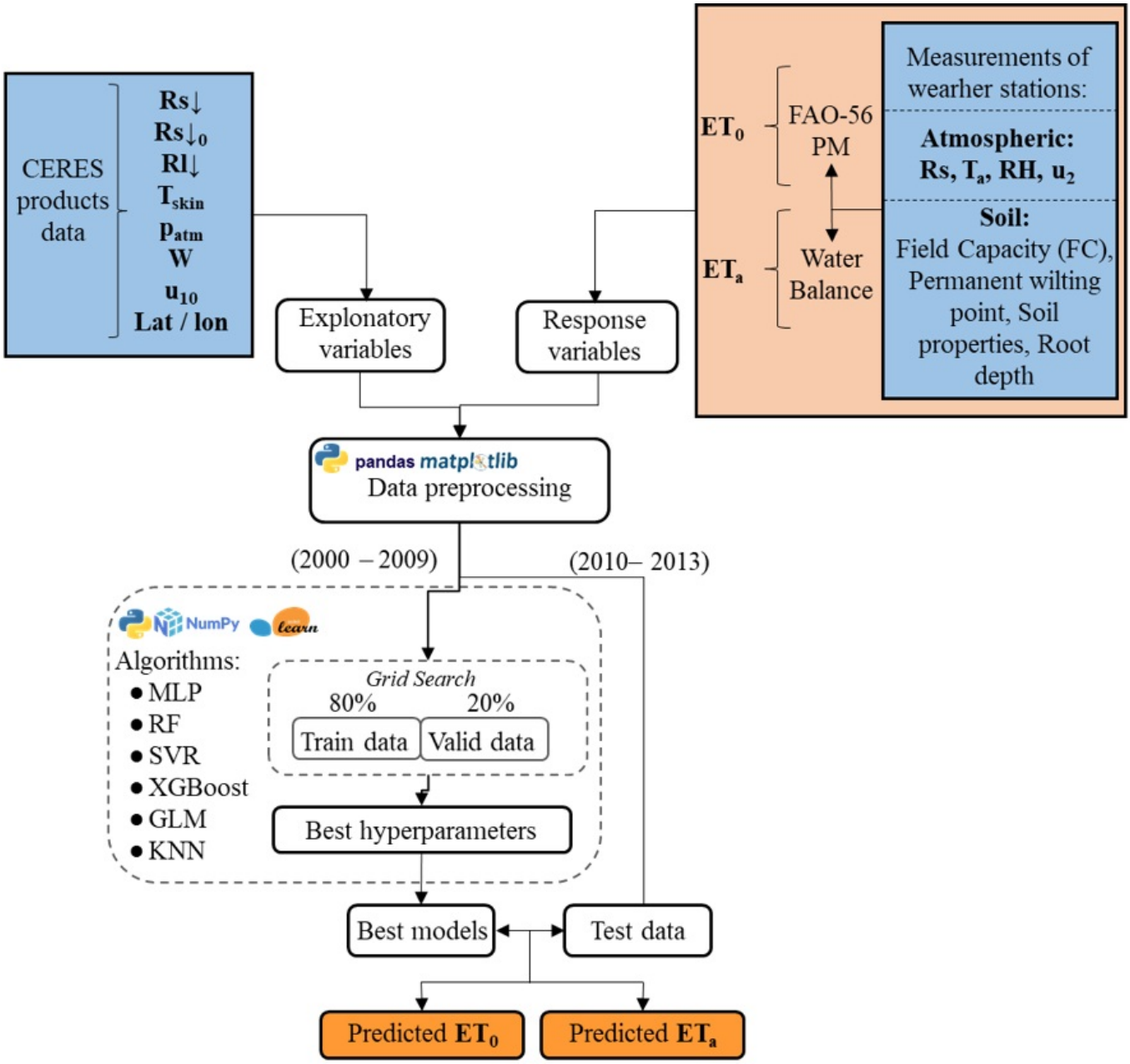

Figure 2: Flow chart of ET_0 and ET_a models. The data processing is shown, where from the exploratory and response variables the predictive models are obtained.

MAE is another useful measure widely used in model evaluations. While they have both been used to assess models' performance for many years, there is no consensus on the most appropriate metric for model errors. While the MAE gives the same weight to all errors, the RMSE penalizes variance as it gives errors with larger absolute values (Chai and Draxler, 2014). While both statistics were used as made by other researchers in similar studies (and we consider both so that the results obtained are easily comparable with those other studies), RMSE was selected for comparing the errors between different algorithms due that RMSE penalizes larger errors more severely, and usually is better at revealing models performance differences. Finally, the coefficient of determination (R^2) was used to show the goodness of fit.

3. RESULTS AND DISCUSSION

3.1. Evaluation of machine learning algorithms

In the Experiment (a), where $Rs_{\downarrow}$, $Rl_{\downarrow}$, and T_{skin} CERES products were considered as input variables to predict ET_0, the MLP model shows the best results with MAE = 0.556 mm d^{-1}, RMSE = 0.749 mm d^{-1}, and R^2= 0.826 (Figure 3a). In contrast, the RF model shows the worst results, with MAE = 0.578 mm d^{-1}, RMSE = 0.784 mm d^{-1}, and R^2= 0.809 over validation dataset.

In the second Experiment (b), where W, p_{atm} and u_{10} CERES products were incorporated as input variables, the statistical errors (MAE and RMSE) decreased between 8 and 15 %. Furthermore, an improvement in 3 to 5 % accuracy was evidenced. In this case, the SVR shows the best results with MAE = 0.505 mm d^{-1}, RMSE = 0.679 mm d^{-1}, and R^2= 0.857.

In the Experiment (c), the theoretical solar radiation is incorporated as an input variable. In this case, all the models improved their performance. Similarly, the SVR also shows the best results in the validation, with MAE, RMSE and R^2 of 0.478 mm d^{-1}, RMSE = 0.659 mm d^{-1}, and R^2= 0.865, respectively.

Finally, in Experiment (d), all models improve their performance by including the location (latitude and longitude) as input variables. The SVR shows the best statistical results when comparing the ET_0 predicted values with those calculated using the PM-FAO56 method (MAE = 0.444 mm d^{-1}, RMSE = 0.609 mm d^{-1}, and R^2= 0.885). Comparing the results of the Experiments (a) and (d), we observed that statistical errors decreased from 14 to 29 %, and the accuracy improved from 4 to 8 %.

For the prediction of ET_a, the machine learning algorithms were trained similarly to the ET_0 models. The MLP model following the experiment a) also shows the best results with MAE = 0.460 mm d^{-1}, RMSE = 0.630 mm d^{-1}, and R^2 = 0.560 (Figure 3b). With more input variables, both RF and SVR were ranked as the best algorithms in the following experiments. The SVR machine-learning model showed statistical values of MAE = 0.400 mm d^{-1}, RMSE = 0.562 mm d^{-1}, and R^2 = 0.650 for the Experiment (d).

It is interesting to note that the performances of RF, SVR and KNN models improve significantly as more input variables are incorporated into the training process. Contrary, the GLM algorithm only is suitable when the number of variables is low (Experiment (a)). Concerning actual evapotranspiration, the GLM model improves its statistical errors by ∼5 %, while, for example, RF improves by up to 20 % by adding more input variables. Table 3 presents a statistical summary of the results obtained in the four experiments with the six machine learning algorithms over the validation dataset, while Figure 3 show a ranking of the models considering the accuracy for each experiment.

Fig. 4 shows the comparisons between ET_0 predicted values with machine learning algorithms (Experiment (d)) and those values obtained using the PM-FAO56 method. Similarly, Fig. 5 shows the comparisons between ET_a predicted and those obtained by soil water balance. From Figures 4 and 5, it is possible to observe that all models developed tend to underestimate both the reference and actual evapotranspiration for higher ET values (ET_0 > 6 mm d^{-1}, and ET_a > 3 mm d^{-1}). However, this characteristic is more evident in the GLM model. The SVR, RF and MLP models generally show better performance, and we found that these have a more remarkable ability to predict evapotranspiration with CERES data.

3.2. Final testing and complementary analysis

After training and validating the algorithms with the daily data set between 2000 and

Experiment	CERES input variables	Algorithm	ET_0 MAE (mm d^{-1})	ET_0 RMSE (mm d^{-1})	ET_0 R^2 (-)	ET_a MAE (mm d^{-1})	ET_a RMSE (mm d^{-1})	ET_a R^2 (-)
(a)	$Rs_{\downarrow}$, $Rl_{\downarrow}$, and T_{skin}	MLP	0.556	0.749	0.826	0.460	0.630	0.560
		RF	0.578	0.784	0.809	0.480	0.656	0.524
		SVR	0.578	0.757	0.822	0.459	0.631	0.559
		XGBR	0.554	0.752	0.824	0.464	0.632	0.557
		GLM	0.576	0.771	0.815	0.475	0.645	0.539
		KNN	0.575	0.781	0.811	0.480	0.655	0.525
Mean			**0.570**	**0.766**	**0.818**	**0.470**	**0.641**	**0.544**
SD			**0.012**	**0.015**	**0.007**	**0.010**	**0.012**	**0.017**
(b)	$Rs_{\downarrow}$, $Rl_{\downarrow}$, T_{skin}, p_{atm}, W, and u_{10}	MLP	0.504	0.692	0.852	0.450	0.622	0.572
		RF	0.505	0.692	0.851	0.444	0.611	0.586
		SVR	0.505	0.679	0.857	0.437	0.609	0.589
		XGBR	0.507	0.693	0.851	0.449	0.616	0.580
		GLM	0.531	0.717	0.840	0.464	0.634	0.555
		KNN	0.515	0.707	0.845	0.455	0.628	0.563
Mean			**0.511**	**0.697**	**0.849**	**0.450**	**0.620**	**0.574**
SD			**0.011**	**0.013**	**0.006**	**0.009**	**0.010**	**0.013**
(c)	$Rs_{\downarrow}$, $Rs_{\downarrow 0}$, $Rl_{\downarrow}$, T_{skin}, p_{atm}, W, and u_{10}	MLP	0.486	0.674	0.859	0.437	0.610	0.588
		RF	0.478	0.662	0.864	0.427	0.595	0.608
		SVR	0.478	0.659	0.865	0.427	0.598	0.603
		XGBR	0.487	0.674	0.859	0.437	0.606	0.594
		GLM	0.518	0.705	0.846	0.454	0.624	0.569
		KNN	0.492	0.683	0.855	0.443	0.617	0.578
Mean			**0.490**	**0.676**	**0.858**	**0.437**	**0.608**	**0.590**
SD			**0.015**	**0.017**	**0.007**	**0.010**	**0.011**	**0.015**
(d)	$Rs_{\downarrow}$, $Rs_{\downarrow 0}$, $Rl_{\downarrow}$, T_{skin}, p_{atm}, W, u_{10}, *lat*, and *lon*	MLP	0.439	0.619	0.881	0.411	0.575	0.634
		RF	0.444	0.621	0.880	0.401	0.562	0.650
		SVR	0.444	0.609	0.885	0.400	0.562	0.650
		XGBR	0.460	0.642	0.872	0.420	0.580	0.627
		GLM	0.506	0.688	0.853	0.452	0.622	0.572
		KNN	0.448	0.629	0.877	0.415	0.580	0.627
Mean			**0.457**	**0.634**	**0.875**	**0.417**	**0.580**	**0.627**
SD			**0.025**	**0.028**	**0.011**	**0.019**	**0.022**	**0.029**

Table III: Performance comparison of the machine learning algorithms over validation dataset. Experiments (a) – (d), where the input variables used are shown. SD: Standard deviation.

2009, we observed that SVR model show the best results, and RF and MLP models have almost similar performances. Therefore, as a complementary analysis, we take the best developed model (SVR for both reference and actual evapotranspiration) to analyze the statistics errors using the independent testing dataset (2010-2013) into different data subsets considering the different climate zones. Table 4 shows the results obtained.

In Carmona et al. (2018), Priestley-Taylor (PT) and PM FAO56 equations were adapted to predict the reference evapotranspiration with CERES data. Its results were between 0.6 - 0.8 mm d^{-1}, 0.8-1.1 mm d^{-1}, and 0.769-0.783 for MAE, RMSE, and R^2, respectively. In this novel study, statistical errors were significantly improved when using machine learning algorithms. We observed that the ML algorithms are better coupled to local conditions than classical models. For predicting

Climate zone	N (n)	daily ET_0			daily ET_a		
		MAE (mm d^{-1})	RMSE (mm d^{-1})	R^2 (-)	MAE (mm d^{-1})	RMSE (mm d^{-1})	R^2 (-)
C	4188 (3)	0.519	0.730	0.866	0.438	0.628	0.626
ST	1396 (1)	0.390	0.556	0.910	0.413	0.576	0.624
THVH	4038 (3)	0.437	0.613	0.891	0.428	0.613	0.595
TO	6888 (5)	0.317	0.447	0.926	0.357	0.518	0.669
TVH	8294 (6)	0.401	0.551	0.912	0.475	0.680	0.580
WHPH	4140 (3)	0.558	0.804	0.850	0.434	0.614	0.587
WH	3851 (3)	0.438	0.607	0.893	0.407	0.563	0.617
Mean		**0.437**	**0.616**	**0.893**	**0.422**	**0.599**	**0.614**
SD		**0.075**	**0.110**	**0.025**	**0.033**	**0.048**	**0.028**

Table IV: Performance of the best-trained machine learning algorithms (for both reference and actual evapotranspiration) in the different climate zones considering the Test dataset. N: number of daily values, n: number of validation sites in each climate zone.

the reference evapotranspiration, we observed mean statistical errors over the Test data set of 0.437 mm d^{-1}, 0.616 mm d^{-1}, and 0.893 for the MAE, RMSE, and R^2, respectively. Deviations of MAE and RMSE values of ∼20 % were observed for the different climate zones. The best results were obtained in the TO zone.

TO zone is the wettest zone, the second windiest, and where wet and dry events of low intensity and long duration are common (Aliaga et al., 2017). This good performance can be explained because the ET is closer to potential rates in the TO zone, with T_{skin} (used as input variable) close to air temperature (required in ET_0). On the other hand, the climate zones of the western of the PRA (C and WHPH) showed higher statistics errors.

In predicting ET_a, we observed mean statistical errors over the Test data set of 0.422 mm d^{-1}, 0.599 mm d^{-1}, and 0.614 for the MAE, RMSE, and R^2, respectively. Also, the best results were obtained in the TO zone. However, worse statistics values were observed in TVH zone (centre location of the PRA). Bohn et al. (2020) observed that this zone has different hydrogeological characteristics related to the errors indicated in our work. We suggest that the water table can generate effects on the difference in evapotranspiration (mainly recent evapotranspiration) according to the climatic cycle, which would affect the process, increasing the error and the difference between the errors of ET_0 and ET_a.

It is helpful to contrast our results concerning other backgrounds regarding the estimation of ET by satellite data in the PRA. For example, Rivas and Caselles (2004) proposed and evaluated a simplified equation to estimate spatial reference evapotranspiration from remote sensing-based surface temperature. Its results were analyzed using 58 NOAA-AVHRR images of the TO zone and showed errors of 0.60 mm d^{-1}. Rivas and Carmona (2013) applied a semi-empirical model to estimate ET_a over pasture and soybean using LandSat satellite images and meteorological observations in Tandil (TO zone). The observed errors for pasture and soybean were 0.98 mm d^{-1} and 1.40 mm d^{-1}. Marini et al. (2017) used regression analysis between MODIS products (Land Surface Temperature and Normalized Difference vegetation Index - NDVI) and information from meteorological stations for

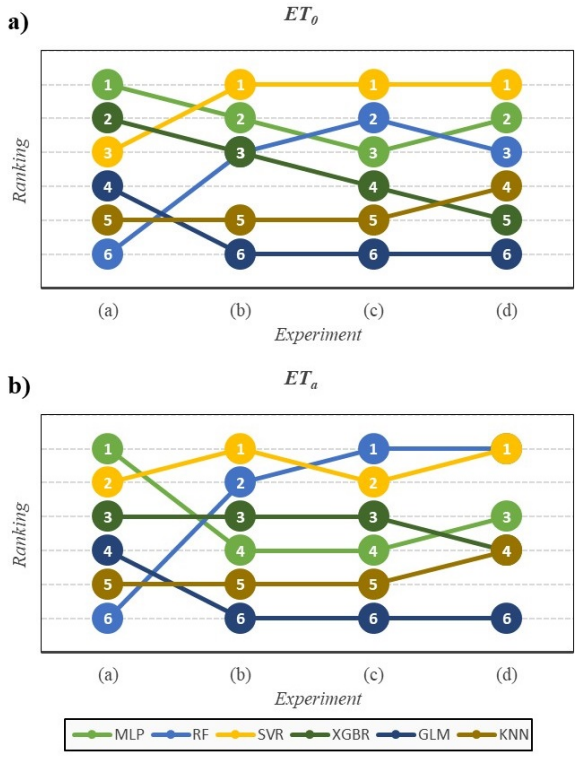

Figure 3: Ranking of the algorithms used in the different experiments ((a) - (d)) considering the RMSE values. a) Ranking of the machine learning algorithms to predict ET_0, and b) Ranking of the machine learning algorithms to predict ET_a.

estimating the evapotranspiration in the southwest of the Buenos Aires Province (Argentina). Its results showed values of R^2 of 0.696 and 0.841 to predict ET_0, and ET_a, respectively. More recently, Walker et al. (2018) presented a formulation to derive the actual evapotranspiration from in situ and microwave data. Its model was calibrated with observed data in the Southern Great Plains – USA (SGP) area (RMSE = 0.88 mm d^{-1}, and R^2 = 0.80) and then was applied in a highly humid period in the PRA with results near to potential rates (RMSE = 1.6 mm d^{-1} comparing the model with potential evapotranspiration values of corresponding to three sites of warm and warm-humid zones).

In addition, to evaluating the models on a daily scale, it is helpful to show the statistical errors of the trained models on other commonly used time scales. We evaluated the statistical errors of the best model for time averaged data every 8, 16 and 30 days. This time resolution also allows us to compare the results obtained with other models evaluated in the PRA. Analyzing of 8 and 16 days averaged data are interesting since they allow the comparison with ET products from satellite sensors with better spatial resolution, such as MODIS products (with spatial resolution between 250 m and 1 km). Table 5 shows the performance metrics at different temporal scales. We observed that the RMSE is about 0.30 mm d^{-1} considering the mean monthly for the ET_0 prediction, while the RMSE is around 0.44 mm d^{-1} for ET_a.

The ET_0 monthly errors obtained in this study were significantly better than those observed in Carmona et al. (2018), who reflect values between 0.37 - 0.53 mm d^{-1}, and 0.47 - 0.64 mm d^{-1} for MAE, and RMSE, respectively, and 0.916 - 0.936 for R^2. On the other hand, Degano et al. (2019) evaluated the correspondence between MOD16A2 product (Mu et al., 2013) and reference evapotranspiration in PRA. Their results showed a systematic overestimation of MOD16A2 product, with RMSE = 2.4 mm d^{-1} and R^2 = 0.86. Subsequently, Degano et al. (2021) corrected the systematic errors of the MOD16A2 products and then evaluated the actual evapotranspiration on extensive soybean crops in the PRA. The statistical errors for predicting the actual evapotranspiration for 8 days- MODIS products on soybean showed 0.44 mm d^{-1}, 0.58 mm d^{-1}, and 0.85 for MAE, RMSE, and R^2, respectively. The performance obtained in this work is comparable to those obtained with more complex and higher spatial resolution satellite products.

4. CONCLUSIONS

In this study, there were developed and evaluated different machine learning models to predict reference and actual evapotranspiration

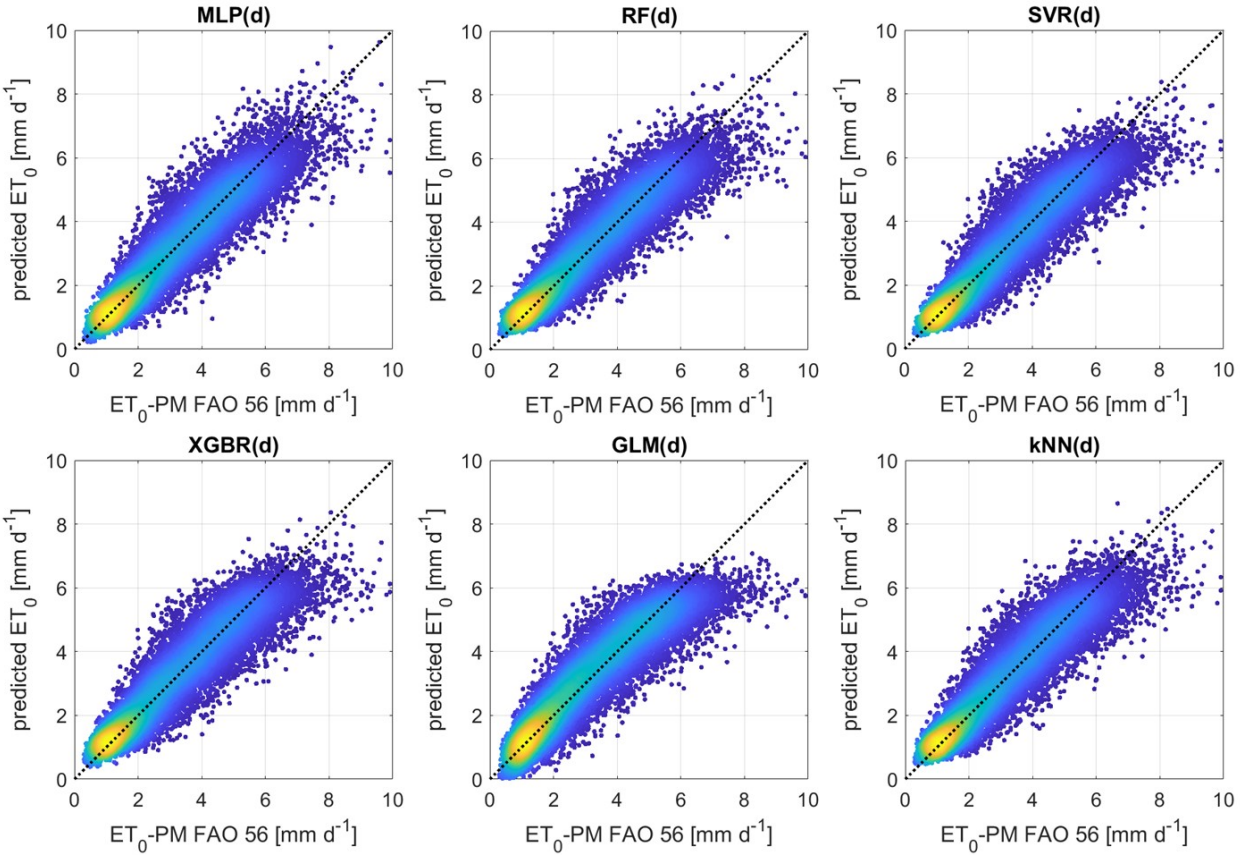

Figure 4: ET_0 models, Experiment (d): predicted ET_0 values versus those obtained with ET_0 PM-FAO56 method over Validation dataset.

		ET₀			***ETₐ***	
Temporal scale (d)	MAE (mm d^{-1})	RMSE (mm d^{-1})	R^2 (-)	MAE (mm d^{-1})	RMSE (mm d^{-1})	R^2 (-)
8	0.266	0.371	0.951	0.354	0.507	0.683
16	0.237	0.329	0.960	0.334	0.477	0.705
30	0.217	0.299	0.966	0.310	0.439	0.733

Table V: Performance of the best-trained machine learning algorithms considering average values every 8, 16 and 30 days on Test dataset.

using different set of CERES satellite products as input. Multilayer Perceptron (MLP), Random Forest (RF), Support vector machine-based regressor (SVR), XGBoost regressor (XGBR), Generalized Linear Models (GLM), and K-neighbors regressor (KNN) machine learning algorithms were used to trained the models and then were compared with ground observations corresponding to agro-meteorological stations distributed in seven climate zones of the Pampean Region of Argentina. The accuracy of the models based on the considered algorithms using different CERES datasets was analyzed. In general, it was observed that the performance of the models increase as more input variables from CERES are included. We observed that the SVR model shows the best performance. The

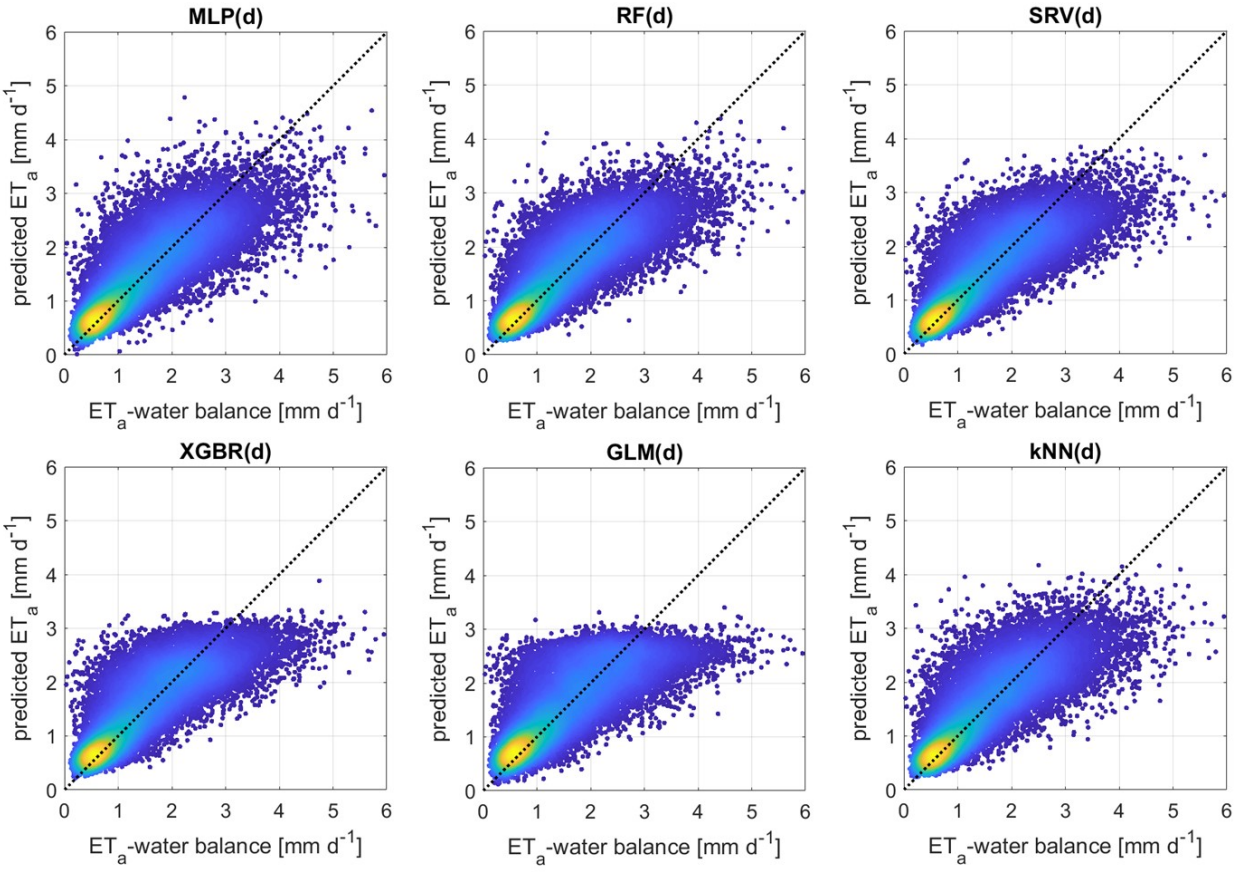

Figure 5: ET_a models, Experiment (d): predicted ET_a values versus those obtained with daily water balance over Validation dataset.

RF and MLP models present almost similar performances than SRV although with a slightly worse accuracy. Then, the best SVR model was analyzed by mean of statistical metrics over the study area using an independent dataset (2010-2013). For the prediction of the reference evapotranspiration, we observed metrics of 0.437 ± 0.075 mm d^{-1}, 0.616 ± 0.110 mm d^{-1}, and 0.893 ± 0.025 for the MAE, RMSE, and R^2, respectively. On the other hand, in predicting actual evapotranspiration, we observed metrics of 0.422 ± 0.033 mm d^{-1}, 0.599 ± 0.048 mm d^{-1}, and 0.614 ± 0.028 for the MAE, RMSE, and R^2, respectively. Furthermore, the statistical metrics were analyzed considering different temporal scales (averaged 8, 16 and 30 days), which allow drawing a baseline to later develop more robust products by incorporating reanalysis products such as MERRA2 and satellite information from MODIS, Landsat or Sentinel images, among others. Comparing the results obtained in this work with other machine learning models to estimate reference evapotranspiration developed by other authors, we understand that our results are promising and represent a baseline for future studies. The combination of CERES variables with information from other sources may generate more specific evapotranspiration products, considering the different land covers.

Acknowledgements: This work was supported by the Consejo Nacional de Investigaciones Científicas y Técnicas (PROG. COOP. BILATERAL LEVEL 1 CONICET - NSFC, 2017, Resol.2018-308- APN-CIR#CONICET). Also, we thank BA. Adriana Basualdo of the Oficina de Riesgo Agropecuario for providing the reference evapotranspiration data and the

terms of daily water balance for the validation sites. The CERES data were obtained from the Atmospheric Science Data Center at NASA Langley Research Center.

REFERENCES

Abbe, E., Bengio, S., Cornacchia, E., Kleinberg, J., Lotfi, A., Raghu, M., Zhang, C., 2022. Learning to Reason with Neural Networks: Generalization, Unseen Data and Boolean Measures (No. arXiv:2205.13647). arXiv. https://doi.org/10.48550/arXiv.2205.13647

Aliaga, V. S., Ferrelli, F., & Piccolo, M. C., 2017. Regionalization of climate over the Argentine Pampas. International Journal of Climatology, 37, 1237–1247.

Allen, R.G., Pereira, L.S., Raes, D., Smith, M., 1998. Crop evapotranspiration: Guidelines for computing crop water requirements. Irrigation and Drainage Paper No 56. Food and Agriculture Organization of the United Nations (FAO), Rome, Italy.

Allen, R.G., Pereira, L.S., Howell, T.A., Jensen, M.E., 2011. Evapotranspiration information reporting: I. Factors governing measurement accuracy. Agric. Wat. Manag. 98 (6), 899–920. https://doi.org/10.1016/j.agwat.2010.12.015.

Bohn V., Rivas R., Varni M., Piccolo C., 2020. Using SPEI in predicting water table dynamics in Argentinian plains. Environmental Earth Sciences 79:469, doi.org/10.1007/s12665-020-09210-0

Breiman, L., 2001. Random Forests. Mach. Learn. 45, 5–32. https://doi.org/10.1023/A:1010933404324

Carmona, F., Holzman, M., Rivas, R., Degano, M.F., Kruse, E., Bayala, M., 2018. Evaluation of two models using CERES data for reference evapotranspiration estimation. Rev. de Teledet. 51, 87–98. https://doi.org/10.4995/raet.2018.9259.

Chen, Z., Shi, R., & Zhang, S., 2013. An artificial neural network approach to estimate evapotranspiration from remote sensing and AmeriFlux data. Frontiers of Earth Science, 7(1), 103–111. https://doi.org/10.1007/s11707-012-0346-7

Chen, T., Guestrin, C., 2016. Xgboost: A scalable tree boosting system, in: Proceedings of the 22nd Acm Sigkdd International Conference on Knowledge Discovery and Data Mining. pp. 785–794.

Chia, M. Y., Huang, Y. F., & Koo, C. H., 2020a. Support vector machine enhanced empirical reference evapotranspiration estimation with limited meteorological parameters. Computers and Electronics in Agriculture, 175, 105577. https://doi.org/10.1016/j.compag.2020.105577

Chai, T. and Draxler, R. R., 2014. Root mean square error (RMSE) or mean absolute error (MAE)? – Arguments against avoiding RMSE in the literature, Geosci. Model Dev., 7, 1247–1250, https://doi.org/10.5194/gmd-7-1247-2014.

Chia, M.Y., Huang, Y.F., Koo, C.H., & Fung, K.F., 2020b. Recent Advances in Evapotranspiration Estimation Using Artificial Intelligence Approaches with a Focus on Hybridization Techniques—A Review. Agronomy, 10(1), 101. https://doi.org/10.3390/agronomy10010101

da Silva Júnior, J.C., Medeiros, V., Garrozi, C., Montenegro, A., Gonçalves, G.E., 2019. Random forest techniques for spatial interpolation of evapotranspiration data from Brazilian's Northeast. Comput. Electron. Agric. 166, 105017. https://doi.org/10.1016/j.compag.2019.105017

Degano, M. F., Rivas, R. E., Carmona, F., Niclòs, R., & Sánchez, J. M., 2021. Evaluation of the MOD16A2 evapotranspiration product in an agricultural area of Argentina, the Pampas region. The Egyptian Journal of Remote Sensing and Space Science. 24(2), pp. 319–328. https://doi.org/10.1016/j.ejrs.2020.08.004

Degano, M.F., Rivas, R.E., Sánchez, J.M., Carmona, F., Niclòs, R., 2019. Assessment of the Potential Evapotranspiration MODIS Product Using Ground Measurements in the Pampas. In Proc. IEEE Congreso Bienal de Argentina, 2018, 1-5. https://doi.org/10.1109/ARGENCON.2018.8646143

Fan, J., Wang, X., Wu, L., Zhou, H., Zhang, F.,

Yu, X., Lu, X., Xiang, Y., 2018. Comparison of Support Vector Machine and Extreme Gradient Boosting for predicting daily global solar radiation using temperature and precipitation in humid subtropical climates: A case study in China. Energy Convers. Manag. 164, 102–111. https://doi.org/10.1016/j.enconman.2018.02.087

Faramiñan, A., Rodriguez, P.O., Carmona, F., Holzman, M., Rivas, R., Mancino, C., 2022. Estimation of actual evapotranspiration in barley crop through a generalized linear model. MethodsX 101665. https://doi.org/10.1016/j.mex.2022.101665

Faramiñán, A.M.G., Degano, M.F., Carmona, F., Rodriguez, P.O., 2021. Estimation of actual evapotranspiration using NASA-POWER data and Support Vector Machine, in: 2021 XIX Workshop on Information Processing and Control (RPIC). XIX Workshop on Information Processing and Control (RPIC), pp. 1–5. https://doi.org/10.1109/RPIC53795.2021.9648425

Granata, F. Gargano, R., de Marinis, G., 2020. Artificial intelligence based approaches to evaluate actual evapotranspiration in wetlands. Science of The Total Environment, Vol. 703, 2020, 135653, ISSN 0048-9697, https://doi.org/10.1016/j.scitotenv.2019.135653.

Han, Y., Wu, J., Zhai, B., Pan, Y., Huang, G., Wu, L., Zeng, W., 2019. Coupling a Bat Algorithm with XGBoost to Estimate Reference Evapotranspiration in the Arid and Semiarid Regions of China. Adv. Meteorol. 2019, e9575782. https://doi.org/10.1155/2019/9575782

Izadifar, Z., Elshorbagy, A., 2010. Prediction of hourly actual evapotranspiration using neural networks, genetic programming, and statistical models. Hydrol. Process. 24, 3413–3425. https://doi.org/10.1002/hyp.7771

Jia, A., Jiang, B., Liang, S., Zhang, X., Ma, H., 2016. Validation and Spatiotemporal Analysis of CERES Surface Net Radiation Product. Remote Sens., 8, 90. https://doi.org/10.3390/rs8020090

Jing, W., Yaseen, Z.M., Shahid, S., Saggi, M.K., Tao, H., Kisi, O., Salih, S.Q., Al-Ansari, N., Chau, K.-W., 2019. Implementation of evolutionary computing models for reference evapotranspiration modeling: short review, assessment and possible future research directions. Eng. Appl. Comput. Fluid Mech. 13, 811–823.

Kisi, O., 2007. Evapotranspiration modelling from climatic data using a neural computing technique. Hydrol. Process. Int. J. 21, 1925–1934.

Kisi, O., 2008. The potential of different ANN techniques in evapotranspiration modelling. Hydrol. Process. 22, 2449–2460. https://doi.org/10.1002/hyp.6837

Kisi, O., Cimen, M., 2009. Evapotranspiration modelling using support vector machines. Hydrol. Sci. J.-J. Sci. Hydrol. 54.

Landeras, G., Ortiz-Barredo, A., López, J.J., 2008. Comparison of artificial neural network models and empirical and semi-empirical equations for daily reference evapotranspiration estimation in the Basque Country (Northern Spain). Agric. Water Manag. 95, 553–565.

Lewis, C.S., & Allen, L.N., 2017. Potential crop evapotranspiration and surface evaporation estimates via a gridded weather forcing dataset. Journal of Hydrology, 546, 450–463. https://doi.org/10.1016/j.jhydrol.2016.11.055

Lu, X., Zhuang, Q., 2010. Evaluating evapotranspiration and water-use efficiency of terrestrial ecosystems in the conterminous United States using MODIS and AmeriFlux data. Remote Sensing of Environment, 114(9), 1924–1939. https://doi.org/10.1016/j.rse.2010.04.001

Marini, F., Santamaría, M., Oricchio, P., Di Bella, C.M., Bausaldo, A., 2017. Estimación de la evapotranspiración real (ETR) y de evapotranspiración potencial (ETP) en el sudoeste bonaerense (Argentina) a partir de imágenes MODIS. Revista de Teledetección, 48, 29-41. https://doi.org/10.4995/raet.2017.6743

Martens, B., de Jeu, R., Verhoest, N.,

Schuurmans, H., Kleijer, J., Miralles, D., 2018. Towards Estimating Land Evaporation at Field Scales Using GLEAM. Remote Sensing, 10(11), 1720. https://doi.org/10.3390/rs10111720

Miralles, D.G., Holmes, T.R.H., De Jeu, R.A.M., Gash, J.H., Meesters, A.G.C.A., Dolman, A.J., 2011. Global land-surface evaporation estimated from satellite-based observations. Hydrol. Earth Syst. Sci., 15, 453–469.

Mu, Q.Z., Zhao, M.S., Running, SW, 2013. MODIS Global Terrestrial Evapotranspiration (ET) Product (NASA MOD16A2/A3). Algorithm Theoretical Basis Document. Collection 5. Numerical Terradynamic Simulation Group. College of Forestry and Conservation. University of Montana.

NASA/LARC/SD/ASDC (2017). CERES and GEO-Enhanced TOA, Within-Atmosphere and Surface Fluxes, Clouds and Aerosols Daily Terra-Aqua Edition4A [Data set]. NASA Langley Atmospheric Science Data Center DAAC. Retrieved from https://doi.org/10.5067/Terra+Aqua/CERES/SYN1degDay_L3.004A

Nema, M.K., Khare, D., & Chandniha, S.K., 2017. Application of artificial intelligence to estimate the reference evapotranspiration in sub-humid Doon valley. Applied Water Science, 7(7), 3903–3910. https://doi.org/10.1007/s13201-017-0543-3

Ochoa-Sánchez A, Crespo P, Carrillo-Rojas G, Sucozhañay A and Célleri R, 2019. Actual Evapotranspiration in the High Andean Grasslands: A Comparison of Measurement and Estimation Methods. Front. Earth Sci. 7:55. https://doi.org/10.3389/feart.2019.00055

Ok, A.O., Akar, O., Gungor, O., 2012. Evaluation of random forest method for agricultural crop classification. Eur. J. Remote Sens. 45, 421–432. https://doi.org/10.5721/EuJRS20124535

Putatunda, S., Rama, K., 2018. A Comparative Analysis of Hyperopt as Against Other Approaches for Hyper-Parameter Optimization of XGBoost, in: Proceedings of the 2018 International Conference on Signal Processing and Machine Learning - SPML '18. Presented at the the 2018 International Conference, ACM Press, Shanghai, China, pp. 6–10. https://doi.org/10.1145/3297067.3297080

Pedregosa, F., Varoquaux, G., Gramfort, A., Michel, V., Thirion, B., Grisel, O., Blondel, M., Prettenhofer, P., Weiss, R., Dubourg, V., Vanderplas, J., Passos, A., Cournapeau, D., Brucher, M., Perrot, M., Duchesnay, É., 2011. Scikit-learn: Machine Learning in Python. Journal of Machine Learning Research, 12(85):28252830, 2011.

Rivas, R., Caselles, V., 2004. A simplified equation to estimate spatial reference evaporation from remote sensing-based surface temperature and local meteorological data. Remote Sens. Environ. 93, 68–76.

Rivas, R.E., Carmona, F. 2013. Evapotranspiration in the Pampean Region using field measurements and satellite data. Physics and Chemistry of the Earth, Parts A/B/C, 55-57, 27-34. https://doi.org/10.1016/j.pce.2010.12.002

Rutan, D.A., S. Kato, D.R. Doelling, F.G. Rose, L.T. Nguyen, T.E. Caldwell, and NG. Loeb, 2015: CERES synoptic product: Methodology and validation of surface radiant flux. J. Atmos. Oceanic Technol., 32, 1121–1143, https://doi.org/10.1175/JTECH-$dˆ-ˆ1$4-00165.1.

Smith, G., Priestley, K., Loeb, N., Wielicki, B., Charlock, T., Minnis, P., Doelling, D., Rutan, D., 2011. Clouds and Earth Radiant Energy System (CERES), a review: Past, present and future. Adv. Space Res., 48, 254–263.

Teyseyre, A., Carmona, F., Holzman, M., Rodriguez, J.M., Schiaffino, S., Rivas, R, Godoy, D., 2021. Evaluating machine learning approaches for evapotranspiration estimation in the Pampean region of Argentina. IEEE Congreso Bienal de Argentina, 2020, pp. 1-7, https://doi.org/10.1109/ARGENCON49523.2020.9505501.

Walker, E., García, G.A.; Venturini, V., 2018. Actual evapotranspiration estimation over flat lands using soil moisture products from

SMAP mission. Revista de Teledetección, n. 52, p. 17-26. ISSN 1988-8740. https://doi.org/10.4995/raet.2018.10566.

Xiang, K., Li, Y., Horton, R., & Feng, H., 2020. Similarity and difference of potential evapotranspiration and reference crop evapotranspiration – a review. Agricultural Water Management, 232, 106043. https://doi.org/10.1016/j.agwat.2020.106043

Yang, F., White, M.A. Michaelis, A.R., Ichii, K., Hashimoto, H., Votava, P., Zhu, A-X, Nemani, RR, 2006. Prediction of Continental-Scale Evapotranspiration by Combining MODIS and AmeriFlux Data Through Support Vector Machine. IEEE Transactions on Geoscience and Remote Sensing, vol. 44, no. 11, pp. 3452-3461. https://doi.org/10.1109/TGRS.2006.876297.

Yamaç, S.S., Todorovic, M., 2020. Estimation of daily potato crop evapotranspiration using three different machine learning algorithms and four scenarios of available meteorological data. Agric. Water Manag. 228, 105875. https://doi.org/10.1016/j.agwat.2019.105875

Zhang, Z., Gong, Y., & Wang, Z., 2018. Accessible remote sensing data based reference evapotranspiration estimation modelling. Agricultural Water Management, 210, 59–69. https://doi.org/10.1016/j.agwat.2018.07.039